EDINBURGH INSTRUMENTS

50 YEARS 1971-2021

RMS1000

RAMAN MICROSCOPE

Extending the capabilities to Photoluminescence Microscopy, Time-Resolved Measurements and Fluorescence Lifetime Imaging (FLIM)

- Truly Confocal
- Five-Position Grating Turrets
- Two Spectrograph Options
- Up to Four Simultaneous Detectors

www.edinst.com

Received: 9 August 2020 | Revised: 9 September 2020 | Accepted: 10 September 2020

DOI: 10.1002/jrs.5999

RESEARCH ARTICLE

Journal of RAMAN SPECTROSCOPY WILEY

228-nm quadrupled quasi-three-level Nd:$GdVO_4$ laser for ultraviolet resonance Raman spectroscopy of explosives and biological molecules

Sergei V. Bykov[1] | **Ryan D. Roppel**[1] | **Michael Mao**[2] | **Sanford A. Asher**[1]

[1]Department of Chemistry, University of Pittsburgh, Pittsburgh, Pennsylvania, USA

[2]Jiangsu Key Laboratory of Advanced Laser Materials and Devices, School of Physics and Electronic Engineering, Jiangsu Normal University, Xuzhou, China

Correspondence
Michael (Guilin) Mao, 101 Shanghai Road, Tongshan New District, Xuzhou, 221116 Jiangsu, China.
Email: michael.mao@uvisir.com

Sanford A. Asher, Department of Chemistry, University of Pittsburgh, Pittsburgh, PA 15260, USA.
Email: asher@pitt.edu

Funding information
ONR, Grant/Award Number: N00014-18-1-2072

Abstract

We describe a new compact diode-pumped solid-state frequency quadrupled quasi-three-level neodymium-doped gadolinium vanadate (Nd:$GdVO_4$) laser that generates ~50 mW of 228-nm quasi-continuous wave light as ns pulses at a tunable kilohertz repetition rate. We developed two generations of this laser. The first generation has a high duty cycle and a tunable repetition rate. The second generation is optimized for maximum output power. We utilize these new lasers to measure ultraviolet resonance Raman (UVRR) spectra of many important chromophores that absorb in deep ultraviolet (UV). We demonstrate the utility of this excitation by measuring the 228-nm absolute differential Raman cross sections of explosives, peptides, aromatic amino acids, and DNA/RNA nucleotides. Deep UV excitation at 228 nm occurs within the $\pi \rightarrow \pi^*$ electronic transitions of these molecules. The 228-nm resonance excitation enhances the Raman intensities of vibrations of NO_x groups, peptide bonds, aromatic amino acid side chains, and DNA/RNA nucleotides. The measured 228-nm UVRR cross sections of these molecules are 10^3–10^4 fold greater than those excited in the visible spectral region. These new lasers should be of great interest for UVRR spectroscopy and for other applications that benefit from compact, high average power deep UV laser light sources with low peak powers.

KEYWORDS

228-nm laser, aromatic amino acid, biomolecule, deep UV resonance Raman spectroscopy, DUV laser, explosive, nucleotide, peptide, protein, UVRR

1 | INTRODUCTION

Ultraviolet resonance Raman (UVRR) spectroscopy is a versatile spectroscopic technique with numerous fundamental and practical applications such as investigating biomolecular structure,[1–4] pharmaceutical and clinical applications,[5,6] forensics applications,[7,8] and trace explosive detection.[9–11]

When the Raman excitation wavelength falls within an electronic transition, the Raman band intensities significantly increase and the Raman spectra can be used for trace chemical analysis.

The UVRR vibrational frequencies provide information on the molecular ground state structure and its environment. The relative enhancement of the different ground state vibrations gives information on the molecular resonant excited state electronic structure and its geometry. The resonance Raman effect enables detection and investigation of the enhanced chemical species at trace levels within complex environments.

Excitation in the deep ultraviolet (DUV) enhances the Raman intensities of many biological molecules such as peptides, proteins, aromatic amino acids, and DNA/RNA nucleotides due to the $\pi \rightarrow \pi^*$ electronic transitions of peptide bonds and the numerous aromatic ring species. Importantly, this enables the enhancement of the Raman intensities of $-NO_x$ groups, which enables the UVRR trace detection of many explosives.

At present, the major barrier for the wide application of UVRR spectroscopy is the lack of inexpensive, compact, energy efficient, and easy-to-use monochromatic DUV light sources. Today, the choice of UVRR excitation below 240 nm is limited to a relatively small set of frequency-converted lasers, and a few solid state, gas, or excimer lasers. Most recently, a few researchers utilized a synchrotron generated tunable DUV light source for UVRR.[12,13]

Our group at the University of Pittsburgh pioneered the development and application of multiple DUV lasers for UVRR spectroscopy. During the early 1980s, Asher and coworkers developed UVRR spectrometers that utilized the frequency doubled and mixed output of dye lasers pumped by the second or third harmonics of Nd:YAG lasers.[14] These dye lasers enabled the first continuously tunable DUV laser sources, with average output powers of tens of milliwatts. Subsequently, we used a higher duty cycle XeCl excimer laser to pump a dye laser in order to decrease the nonlinear optical phenomena common to low duty cycle Nd:YAG lasers.[15]

High repetition rate excimer lasers increased spectral signal-to-noise ratios for UVRR measurements, but the short UV laser dye lifetimes made their maintenance costly and labor intensive. A collaboration with Coherent Inc. in the early 1990s spawned the development of an intracavity doubled Ar^+-ion continuous wave (CW) laser. This laser generated tens to hundreds of milliwatts of CW 257-, 248-, 244-, 238-, and 228.9-nm ultraviolet (UV) light.[16] A few years later, an intracavity doubled Kr^+-ion laser that generated 206.5- and 234-nm light was developed for deep UVRR spectroscopy.[17] These CW lasers are nearly ideal excitation sources for UVRR measurements because the low peak powers minimized nonlinear, optical saturation and the thermal degradation phenomena typically observed for low duty cycle pulsed lasers. The disadvantages of the doubled Ar^+/Kr^+-ion lasers are their limited wavelength tunability, large size, high cost, and low energy efficiency.

One of the first inexpensive and compact DUV lasers was manufactured by Photon Systems Inc. (Covina, CA). This hollow cathode He–Ag laser generated ~2 mW of quasi-CW 224.3-nm light.[18] One of the remarkable features of the hollow cathode lasers is their ability to operate in a wide temperature range (from −135°C to +70°C without preheating or temperature regulation). These lasers can also be made vibration and shock resistant. A 248.6-nm Ne–Cu hollow cathode laser made by Photon Systems Inc. will be used in the UVRR spectrometer, SHERLOC, that will be carried aboard the 2020 NASA Mars exploration rover "Perseverance."[19]

In 2005, we constructed a DUV Raman spectrometer that utilized the quadrupled output of Ti-sapphire lasers.[20] The combination of continuous wavelength tunability between 193 and 240 nm, high average power, and high repetition rates makes this laser an excellent excitation source for UVRR measurements.

Most recently, Spectra-Physics Inc. and M Squared Lasers Inc. developed CW high efficiency ring lasers that are continuously tunable from the infrared region down to DUV. These laser light sources will minimize the nonlinear optical phenomena that occur upon UVRR excitation. They can also minimize the sample heating and impact of photochemistry. But these lasers are large, complex, and expensive.

We recently focused on developing relatively inexpensive compact, energy efficient, low maintenance DUV lasers for UVRR and standoff detection applications. In 2015, we collaborated with UVISIR (Beachwood, OH) to develop a new compact acousto-optically Q-switched diode-pumped solid-state (DPSS) intracavity frequency-tripled Nd:YVO_4 laser capable of producing ~100 mW of quasi-CW 213-nm light.[21] This laser was successively used for standoff UV Raman spectral measurements for trace explosives detection.

In the work here, we describe a new compact 228-nm quasi-CW, quasi-three-level, frequency-quadrupled Nd:$GdVO_4$ laser as a new excitation source for UVRR. We demonstrate high S/N 228-nm UVRR measurements of peptides, proteins, aromatic amino acids, DNA/RNA nucleotides, and explosives.

2 | DEVELOPMENT OF NEW 228-NM LASER

2.1 | Gain medium

The 228-nm laser gain medium is a neodymium-doped gadolinium vanadate crystal. This is an ideal laser gain medium for a compact DPSS laser system because of its high emission cross section and slope efficiency, excellent thermal conductivity, low lasing threshold, and its high laser damage threshold. The Nd:$GdVO_4$ crystals were first introduced as gain medium in 1992.[22] The degeneracy of the upper Nd:$GdVO_4$ lasing levels results in fewer emission transitions that serves to increase its stimulated emission cross section.[23,24] The $GdVO_4$ crystals have a

high thermal conductivity, similar to the Nd:YAG crystals,[25] that gives rise to excellent heat dissipation. The Nd:$GdVO_4$ crystals also have broad absorption band (~80% broader than Nd:YAG) and large absorption coefficient for our ~808-nm pump wavelength (approximately seven times greater than Nd:YAG at the same neodymium concentration).[23]

The operational temperature of the DPSS laser pump diodes must be maintained within a narrow range because the diode emission wavelengths are temperature dependent. They typically redshift by ~0.3 nm/°C in response to changes in the thermal population of the diode energy levels. The broad absorption of the Nd:$GdVO_4$ crystal[23,24] decreases the requirements for the pump diode emission wavelength stability, simplifying the laser temperature control requirements.

2.2 | Reabsorption phenomenon in the quasi-three-level Nd:$GdVO_4$ laser

To generate 228-nm UV lasing, we quadrupled the 912-nm fundamental of the quasi-three-level laser. This 912-nm lasing transition arises from the $^4F_{3/2} \rightarrow {}^4I_{9/2}$ transition of the Nd^{3+} ions in the $GdVO_4$ crystal.

Figure 1 compares the energy level diagram of the conventional Nd:$GdVO_4$ four-level laser (1063 nm) to the quasi-three-level laser that generates 912-nm lasing.

In the four-level laser, neodymium ions are excited by 808-nm light from the ground state to a short lifetime, higher energy level through the $^4I_{9/2} \rightarrow {}^4F_{5/2}$ transition. Then the Nd^{3+} radiationlessly relaxes to an upper lasing level through the $^4F_{5/2} \rightarrow {}^4F_{3/2}$ transition. After the 1063-nm lasing transition $^4F_{3/2} \rightarrow {}^4I_{11/2}$, the lower lasing level quickly relaxes due to nonradiative transitions to the ground state, $^4I_{11/2} \rightarrow {}^4I_{9/2}$. This fast nonradiative relaxation prevents 1063-nm light reabsorption in the four-level laser system.

In contrast, in the quasi-three-level laser, the 912-nm lasing transition occurs from $^4F_{3/2}$ to the highest sublevel of a crystal field split ground state manifold $^4I_{9/2}$. This highest sublevel of $^4I_{9/2}$ is partially populated at room temperature due to thermal equilibration. This creates conditions for the laser light reabsorption, where the gain medium emits and absorbs at the same wavelength. This reabsorption can significantly decrease the lasing efficiency. The negative impact of this reabsorption can be minimized by optimizing the Nd^{3+} concentration, the Nd:$GdVO_4$ crystal length, the pump beam divergence, and the transmission of the output coupling mirror.[26] We can also suppress reabsorption by cooling the Nd:$GdVO_4$ crystal. Cooling decreases the population of the highest sublevel of the crystal field split ground state $^4I_{9/2}$.[27] Decreasing the temperature of the quasi-three-level laser gain medium gradually converts it into a four-level laser gain medium.

2.3 | 228-nm laser designs

We developed two generations of the 228-nm laser. The first-generation laser has a high duty cycle and a tunable repetition rate. High duty cycle laser excitation can be used to minimize sample photochemistry and sample thermal degradation. It can also minimize Raman saturation and other nonlinear phenomena.[15] Tunable laser repetition rates are desirable for many spectral techniques such as standoff photoacoustic spectroscopy.[28]

Our second-generation 228-nm laser was miniaturized and optimized to achieve maximum output powers.

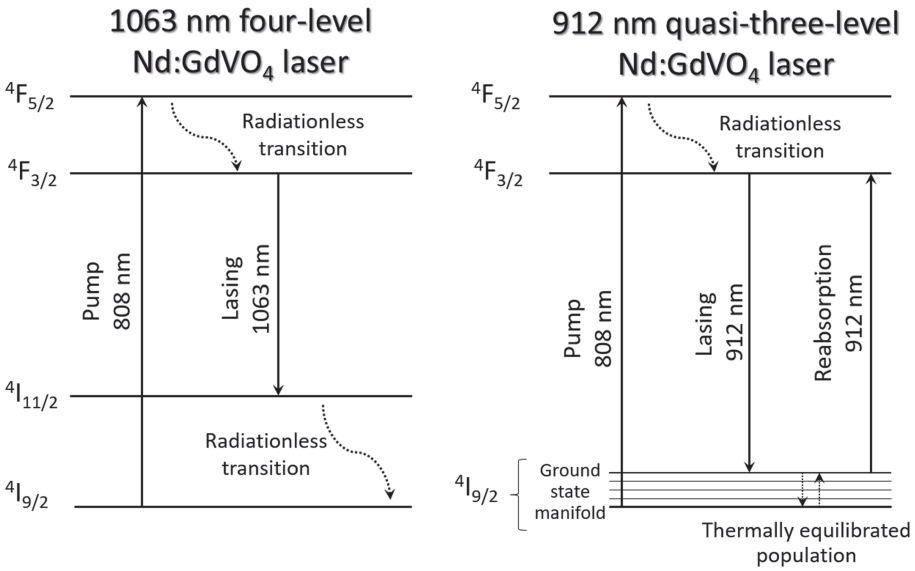

FIGURE 1 Simplified energy level diagram of Nd^{3+} ions in $GdVO_4$ host crystal displays four-level (1063 nm) and quasi-three-level (912 nm) lasing transitions. Only levels that participate in lasing are shown

The development of this second-generation 228-nm laser was challenging due to the decreased laser head size that created complex heat dissipation issues. Both lasers were designed and fabricated by UVISIR Inc. (Beachwood, OH).

2.4 | Generation 1 of the 228-nm laser

This is an acousto-optically Q-switched DPSS laser that is frequency quadrupled to 228 nm. It produces up to ~30 mW of 228-nm quasi-CW light as 60 ns pulses delivered at a tunable ~20–40 kHz repetition rate. The laser head size is 50 × 16 × 11 cm. This laser has a power consumption of ~700 W. The laser employs two separate closed-loop cooling systems (water chillers). One chiller maintains a stable temperature for the laser gain medium, whereas the other maintains the second harmonic generation crystal temperature.

Figure 2a shows the optical layout of this tunable repetition rate 228-nm DPSS laser. A 50W 808-nm CW laser diode was used as an optical pump. The laser gain medium is a 3 × 3 × 6 mm Nd:$GdVO_4$ crystal with a Nd^{3+} doping concentration of 0.15%. The gain medium is water cooled to 4°C. Both ends of the crystal are anti-reflection coated for 912-, 1063-, and 1340-nm wavelengths. A high frequency (80 MHz) acousto-optic Q-switch was chosen to ensure a large deflection angle and high laser hold off. The Q-switch repetition rate is tunable between ~20 and 40 kHz. A 3 × 3 × 15 mm type-I lithium triborate (LBO) crystal was used to convert the horizontally polarized 912-nm fundamental to vertically polarized 456-nm light through intracavity second harmonic generation. M3 is a high reflection mirror for both 456- and 912-nm wavelengths. M4 is a dichroic mirror that transmits 456-nm light but reflects 912-nm light. The 456-nm power is ~500 mW. A 5 × 5 × 10 mm type-I β-barium borate (BBO) crystal was used to convert the 456-nm light into horizontally polarized 228-nm light. A pair of Brewster angle prisms separates the 228-nm light from the 456-nm light.

2.5 | Generation 2 of the 228-nm laser

This is an electro-optically Q-switched DPSS laser that is frequency quadrupled to 228 nm. It produces up to ~50 mW of 228-nm light as a train of ~20 ns pulses at a fixed 6-kHz repetition rate. The size of the laser head is 30 × 16 × 11 cm. The power consumption is ~300 W. It utilizes a single ultra-compact closed-loop cooling system.

Figure 2b shows the optical layout of the second generation 228-nm DUV DPSS laser. A 120W 808-nm laser diode was used as a pump source. To minimize the heat load on the Nd:$GdVO_4$ crystal, and to increase gain, the diode was used in a pulsed mode, with a repetition rate of 6 kHz, and a duty cycle of ~30%, which results in an average diode power dissipation of ~40 W. This decreased heat load reduces the reabsorption phenomenon in this quasi-three-level laser system, which increases the overall laser efficiency. It also reduces the required cooling capacity for the Nd:$GdVO_4$ crystal.

The electro-optic Q-switch utilizes a 3 × 3 × 20 mm BBO crystal that is switched by a Pockels cell driver actuated by a ~3.5-kV high-voltage power supply. This electro-optic Q-switch is faster than the acousto-optic one used in our Generation 1 laser. The typical Q-switching time of the acousto-optic Q-switch is ~30 ns whereas that of the electro-optic Q-switch is ~5 ns.

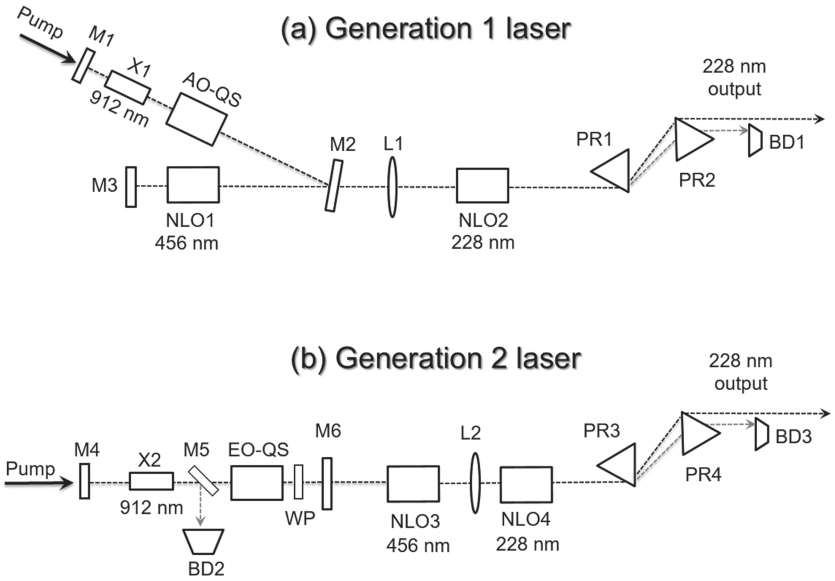

FIGURE 2 Optical layouts of 228-nm lasers. (a) First generation laser is an acousto-optically Q-switched 228-nm DUV laser. M1: pump mirror; X1: Nd:$GdVO_4$ laser crystal; AO-QS: acoustic-optic Q-switch; M2: dielectric mirror; NLO1: LBO crystal; M3: back mirror; L1: lens; NLO2: BBO crystal; PR1, PR2: beam separation prisms; BD1, BD2: beam dumpers. (b) Second generation laser is an electro-optically Q switched 228-nm DUV laser. M4: pump mirror; X2: Nd:$GdVO_4$ laser crystal; M5: polarizer; BD2,BD3: beam dumpers; EO-QS: electro-optic Q-switch, WP: half waveplate, M6: output coupler; NLO3: BiBO crystal, L2: lens, NLO4: BBO crystal, PR3, PR4: prism

The acousto-optic Q-switching mechanism utilizes diffraction of intracavity laser light by the periodic refractive index variation generated by sound waves. The diffracted angle is small. For the short laser cavity of our miniaturized Generation 2 laser, the diffracted light can be amplified. This results in a decreased beam quality and more importantly in an incomplete hold-off and thus unstable laser output.

In contrast, electro-optic Q-switching is based on changing the light polarization via the electro-optic effect. The electro-optic Q-switch performance is independent of the laser cavity length. It results in improved beam quality and enables sharper output pulses. Also, in a miniature laser cavity, faster Q-switching results in shorter laser pulses, which improves the harmonic generation efficiencies.

The Generation 1 laser has a fourth harmonic generation efficiency of ~5%, whereas the second-generation laser has a fourth harmonic generation efficiency of ~20%. The Nd:$GdVO_4$ cavity contains a polarizer, a quarter wave plate, and the electro-optic Q-switch to generate ~600 mW of pulsed 912-nm light. A type-II bismuth borate (BiBO) nonlinear crystal was used to convert the 912-nm laser light to ~200 mW of 456-nm light by extracavity second harmonic generation.

BiBO was chosen because of its larger nonlinear coefficient (d = 3.45 pm/V), which is more than four times larger than that of LBO (d = 0.8 pm/V). A 5 × 5 × 10 type-I BBO crystal was used to generate the 228-nm DUV laser light.

3 | MATERIALS AND METHODS

3.1 | Materials

Solutions of pentaerythritol tetranitrate (PETN) (AccuStandard) and trinitrotoluene (TNT) (AccuStandard) in acetonitrile were evaporated to dryness and reconstituted in deuterated acetonitrile. CD_3CN (Acros Organics) was used both as a solvent and as an internal Raman intensity standard. Solid ammonium nitrate (AN) (JT Baker) was dissolved in a H_2O:CD_3CN (1:1 by volume) mixture due to its low solubility in pure CD_3CN.

Lysozyme (chicken egg white), L-tyrosine (Tyr), L-histidine (His), tri-L-alanine (Ala_3), L-phenylalanine (Phe), L-tryptophan (Trp), 2′-deoxyadenosine 5′-monophosphate (dAMP), 2′-deoxycytidine 5′-monophosphate (dCMP), 2′-deoxyguanosine 5′-monophosphate (dGMP), thymidine 5′monophosphate (dTMP), and 2′-deoxyuridine 5′-monophophoric acid (dUMP) were obtained from Sigma and used without additional purification. Aqueous solutions of the peptides, proteins, amino acids, and mononucleotides contained 0.1-M sodium perchlorate (Sigma) as an internal Raman intensity standard. Minimal HCl (Sigma) was added to completely solubilize solutions of L-tyrosine, L-tryptophan, and L-histidine.

3.2 | Absorption measurements

The absorption spectra of solutions were measured using a Varian Cary 5000 UV-visible-near-infrared spectrometer. All samples were diluted to achieve absorbances <1 in the 200 to 300-nm spectral region.

3.3 | UVRR measurements

We utilized our new 228-nm lasers as the excitation sources for all Raman measurements here. The Raman scattered light was dispersed by a UV-optimized SPEX Triplemate spectrograph described elsewhere.[14] Approximately 3 ml of each ~1 mg/mL sample solution was continuously stirred within a square 1-cm path-length capped, fused silica cuvette (Starna Cells) during the Raman measurements. Typical spectral accumulation times were between 0.4 and 30 s. The spectra were measured using 10–15 mW of 228-nm laser power at the sample focused to a ~100-μm diameter spot.

3.4 | Raman cross section measurements

CD_3CN was used as an internal standard for AN, PETN, and TNT Raman cross section measurements. Specifically, we used the 228-nm absolute differential Raman cross section of the CD_3CN 833 cm^{-1} C–C stretching band, $\sigma_{228}(CD_3CN, 833\ cm^{-1}) = 5.45{\cdot}10^{-29}$ cm^2/molc·sr, which was measured in a 1:1 mixture (by volume) of CD_3CN:CH_3CN. The absolute differential Raman cross sections of CH_3CN can be calculated for any DUV wavelength.[29]

$NaClO_4$ was used as an internal standard for aqueous solution samples of the amino acids, protein, peptide, and DNA/RNA nucleotides. We calculated that the $\sigma_{228}(ClO_4^-, 932\ cm^{-1}) = 6.22{\cdot}10^{-28}$ cm^2/molc·sr using its known wavelength dependence.[29]

Fused silica cuvette Raman contributions were numerically subtracted. Spectral processing and calibrations were performed with the optical spectroscopy software Spectragryph v1.2.11. Peak fitting and integration were done by using GRAMS/AI 8. Absolute differential Raman cross sections were corrected for self-absorption and spectrometer efficiencies as described elsewhere.[30]

4 | UVRR OF EXPLOSIVES AND BIOLOGICAL MOLECULES

Many organic and inorganic molecules show strong DUV absorption bands that give rise to strong resonance enhanced Raman intensities. In the simplest case, we can roughly estimate the excitation wavelength dependence of the resonance Raman intensities by using the Albrecht A term approximation. This expression indicates that the resonance Raman cross sections scale with the square of the molar absorptivity of an isolated resonance excited electronic transition.[31] The magnitude of resonance enhancement increases nonlinearly with the proximity of the excitation frequency to the frequency of the electronic absorption band maximum.

As shown below, excitation close to 228-nm results in strong enhancements of the Raman band intensities for many explosives, peptides, proteins, and nucleic acids.

For the explosive species and the biological compounds discussed below, we see complex broad absorption bands extending from below 200 nm and up to 300 nm. Each absorption spectrum can yield a unique and complex resonance Raman excitation profile. An increase in the complexity arises when these numerous transitions overlap. We also typically observe overlapping contributions from preresonance and resonance Raman excitations that show both homogeneous and inhomogeneous contributions to the excitation profile lineshapes.

Most molecules containing a double bond will have their first $\pi \rightarrow \pi^*$ electronic transition around 200 nm. Upon further conjugation extension, the $\pi \rightarrow \pi^*$ transitions will redshift. Our 228-nm laser is useful for selectively enhancing molecules with relatively small delocalized π electronic systems such as those found in explosives and biological molecules.

4.1 | 228-nm excitation for UVRR of explosives

We previously demonstrated that UVRR is a very sensitive method for the detection of trace explosives.[9,11] Figure 3a shows the DUV absorption spectra of solutions of TNT, PETN, and AN. TNT has at least three overlapping absorption bands with maxima below 200 nm, at ~230 nm and at ~260 nm, due to the $\pi \rightarrow \pi^*$ and $n \rightarrow \pi^*$ transitions of the nitro groups.[32] The 228-nm excitation is in resonance with these transitions, strongly enhancing vibrational modes associated with the TNT nitro groups. Both AN and PETN show absorption maxima deeper in the UV due to the $\pi \rightarrow \pi^*$ transitions of the nitrate or nitrate ester groups.[33,34] The 228-nm excitation is in preresonance with these transitions.

In the 228-nm UVRR spectrum of TNT (Figure 3b), the strongest band at 1354 cm^{-1} derives from the $-NO_2$ symmetric stretching coupled to C–N stretching. The 1549 and 1616 cm^{-1} bands derive from vibrations where the aromatic ring stretching couples to $-NO_2$ asymmetric stretching. The 1209 cm^{-1} band derives from a symmetric aromatic ring breathing motion of the TNT molecule.[30,35] The 228-nm UVRR spectrum of PETN is dominated by vibrations associated with the nitrate ester group ($-ONO_2$). The strongest band is the $-NO_2$ symmetric stretch coupled to CH_2 wagging and CH bending at 1294 cm^{-1}. This is followed by bands at 1510 and 1658 cm^{-1}, which involves CH_2 scissoring and $-NO_2$

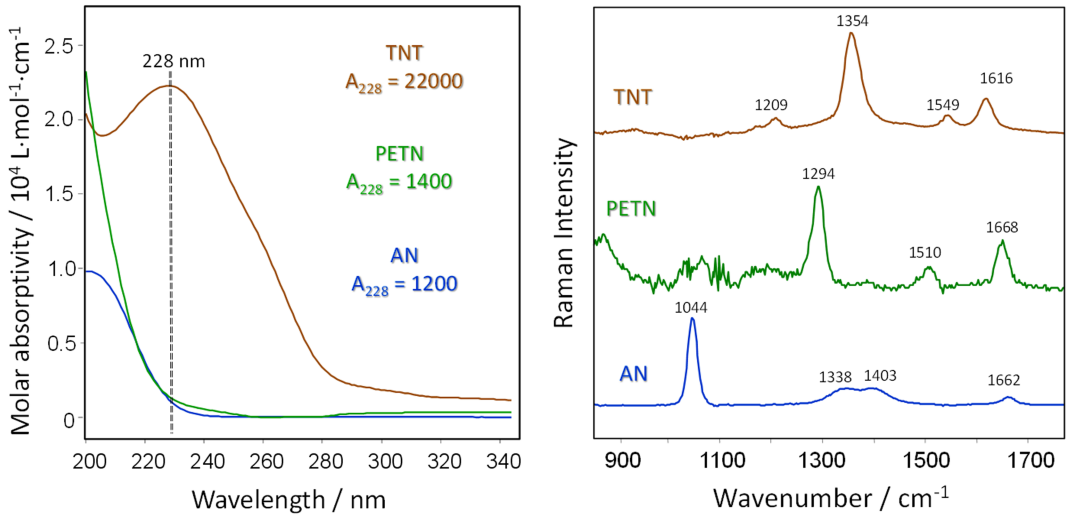

FIGURE 3 (a) DUV absorption spectra of solutions of TNT, PETN and AN. A_{228} indicates the 228-nm solution molar absorptivity. (b) 228-nm UVRR spectra of the explosive solutions shown in Figure 3a: TNT (1 mg/mL in CD_3CN, 20 s accumulation time), PETN (1 mg/mL in CD_3CN, 0.4 s accumulation time), AN (1 mg/mL in CD_3CN/H_2O mixture, 4 s accumulation time) [Colour figure can be viewed at wileyonlinelibrary.com]

asymmetric stretching, respectively.[30,35] The 228-nm UVRR spectrum of AN (Figure 3b) is dominated by the 1044 cm^{-1} (ν_1) nitrate totally symmetric stretching band. Nitrate asymmetric stretches are coupled to water vibrations (ν_3) at ~1338 and 1403 cm^{-1}. Additionally the UVRR show the overtone of the out-of-plane deformation ($2\nu_2$) at ~1662 cm^{-1}.[30,35]

We also measured the 228-nm absolute differential Raman cross sections of TNT, PETN, and AN as shown in Tables S1, S2, and S3.

4.2 | 228-nm UVRR of amino acids, peptides, and proteins

Figure 4a shows the DUV absorption spectra of the aromatic amino acids, which are dominated by the $\pi \rightarrow \pi^*$ transitions of the aromatic rings. Both Trp and Tyr have two absorption maxima, a strong one at ~220 nm and a weak one at ~280 nm. Our 228-nm excitation is close to the strong 220-nm maxima. This results in a maximal enhancement of the in-plane vibrations of the Trp and Tyr aromatic rings.

Our 228-nm excitation is also in preresonance with the His and Phe aromatic rings and with the Ala_3 peptide bond electronic transitions. His and Phe in aqueous solutions show absorption maxima deeper in the UV, at ~210 nm, whereas Ala_3 shows a maximum peptide bond absorbance below 200 nm, due to the $\pi \rightarrow \pi^*$ transitions of the polypeptide backbone.

The UVRR spectrum of Trp (Figure 4b) has three main bands at 758, 1010, and 1550 cm^{-1}, which derive from symmetric stretching of the benzene/pyrrole rings. Tyr shows its most intense band at 1617 cm^{-1} due to phenol in-plane ring stretching. In addition, there are several smaller bands due to aromatic ring stretches coupled to other vibrations.[36]

His, or in our case histidinium, under our acidic conditions, has two intense UVRR bands at 1200 and 1497 cm^{-1} due to coupling of imidazole ring deformation with N–H/C–H bending modes.[37] The UVRR spectrum of Phe has three main bands at 1003, 1207, and 1605 cm^{-1} deriving from aromatic ring stretches coupled to N–H/C–H bendings.[36]

The UVRR spectrum of Ala_3 shows polypeptide backbone vibrations at 1263 (Am III), 1403 (Cα-H), 1536 and 1560 (Am II), and 1670 cm^{-1} (Am I), which are enumerated in terms of particular aide vibrations.

The 228 nm absolute differential Raman cross sections of Trp, Tyr, His, Phe, and Ala_3 are shown in Tables S4-S8 in the supplementary information section.

4.3 | 228-nm UVRR of DNA/RNA nucleotides

Nucleic acids show strong UVRR enhancement when excited in the DUV. Their DUV absorbance derives from their purine and pyrimidine aromatic heterocycles. Each nucleotide shows numerous overlapping $\pi \rightarrow \pi^*$ electronic transitions in the plane of the pyrimidine or purine aromatic rings. Their out-of-plane $n \rightarrow \pi^*$ transitions give rise to much weaker RR enhancements.[38,39]

The absorption spectrum of dCMP shows transitions at ~205, ~215, ~240, and ~270 nm from their pyrimidine chromophore. The absorption spectrum of dAMP

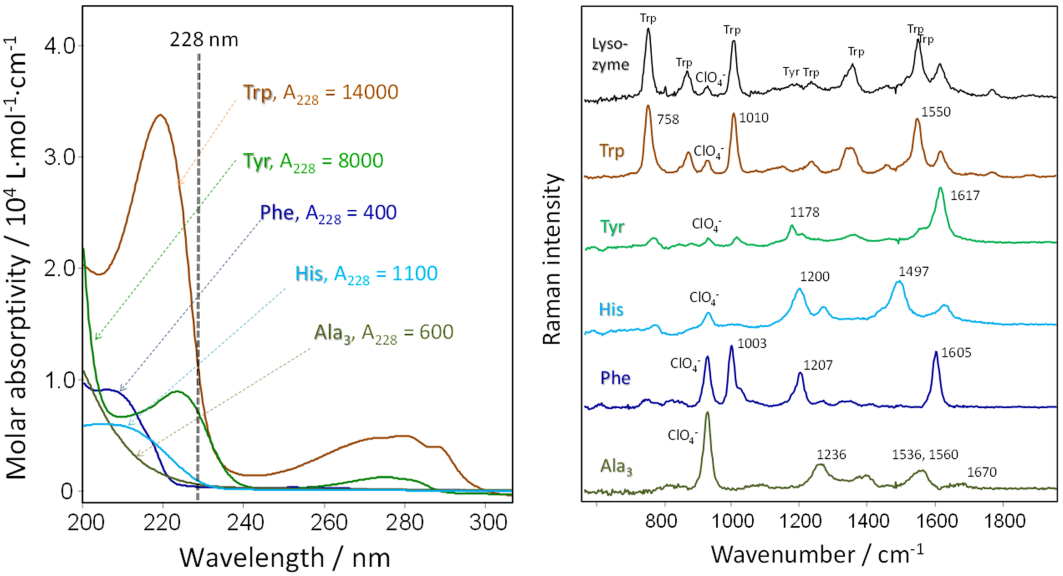

FIGURE 4 (a) DUV absorption and (b) 228-nm Raman spectra (~1 mg/mL, 30 s accumulation time) of aromatic amino acids, peptides and proteins. A_{228} is the molar absorptivity at our 228-nm Raman excitation wavelength [Colour figure can be viewed at wileyonlinelibrary.com]

shows multiple transitions from their purine chromophore at ~200, ~213, ~230, ~245, and ~260 nm. The absorption spectrum of dGMP shows transitions at ~200, ~255, and ~275 nm due its purine chromophore. The absorption spectral features of dUMP and dTMP are similar and show transitions at ~215 and ~265 nm.[40]

228-nm Raman excitation is in resonance with multiple nucleotide transitions. This results in UVRR spectra that show a complex dependence of nucleotide Raman cross sections on the excitation wavelength.

DNA/RNA nucleotide DUV electronic transitions cluster into two absorption spectral regions, low energy, ~260 nm and high energy, at ~200 nm (Figure 5a). In general, the nucleotide Raman band excitation profile cross sections roughly follow the net absorption band shape. However, these excitation profiles generally show a single maximum at either ~260 or ~200 nm.[40–42] Our 228-nm excitation falls at a local absorption minimum between these DUV absorption maxima, leading to a decreased enhancement.

Figure 5b shows aqueous 228-nm UVRR spectra of dAMP, dCMP, dGMP, dTMP, and dUMP; 228-nm excitation enhances neither the sugar nor phosphate vibrations. The UVRR spectra are dominated by the in-plane aromatic ring stretching vibrations.[40] Briefly, dCMP shows the dominantly intense ν_a^6 pyrimidine ring stretch at 1530 cm^{-1}. Two smaller bands at 1647 and 1295 cm^{-1} derive from the C═O/C═C stretching and the glycoside stretching modes. dAMP has an intense ν_a^6 purine ring stretching at 1580 cm^{-1} and a smaller $\nu_{\delta a}^6$ vibration at 1308 cm^{-1}. dGMP has two intense bands at 1365 and 1487 cm^{-1} from $\nu_{\delta b}^6$ and ν_2^5 purine ring stretches and has weaker bands at 1327, 1574, and 1603 cm^{-1} from other purine modes and the NH_2 scissoring modes.[43] dTMP has two intense bands at 1485 and 1653 cm^{-1} from the pyrimidine ring stretches, CH_3 deformations, and C═O/C═C modes and some weaker bands at 785 and 1279 cm^{-1}, also due to the pyrimidine ring stretching modes.[44] The dUMP does not have dominant bands, but shows a series of similarly intense bands at 784, 1234, 1279, 1404, 1478, 1625, and 1686 cm^{-1} from pyrimidine ring modes and C═O/C═C modes.[43]

The 228 nm absolute differential Raman cross sections of dCMP, dAMP, dGMP, dTMP, and dUMP are shown in Tables S9-S13 in the supplementary information section.

4.4 | 228-nm Raman cross sections of explosives, aromatic amino acids, proteins, and DNA/RNA nucleotides

In order to summarize the utility of our new laser, we measured the 228-nm absolute differential Raman cross sections for the explosives (AN, PETN, and TNT) and the aromatic amino acids (Trp, Tyr, His, and Phe). We also measured the peptide Ala_3 and the DNA/RNA nucleotides: dAMP, dCMP, dGMP, dTMP, and dUMP. See the Supporting Information for their cross sections. In general, the 228-nm Raman cross sections show 10^3–10^4 fold greater intensities than those excited in the visible spectral region.[36,43,45] Figure 6 compares the 228-nm cross sections of the most intense Raman bands for these compounds.

Among explosives, TNT demonstrates the highest 228-nm cross section for the 1354 cm^{-1} band, σ_{228}(TNT,

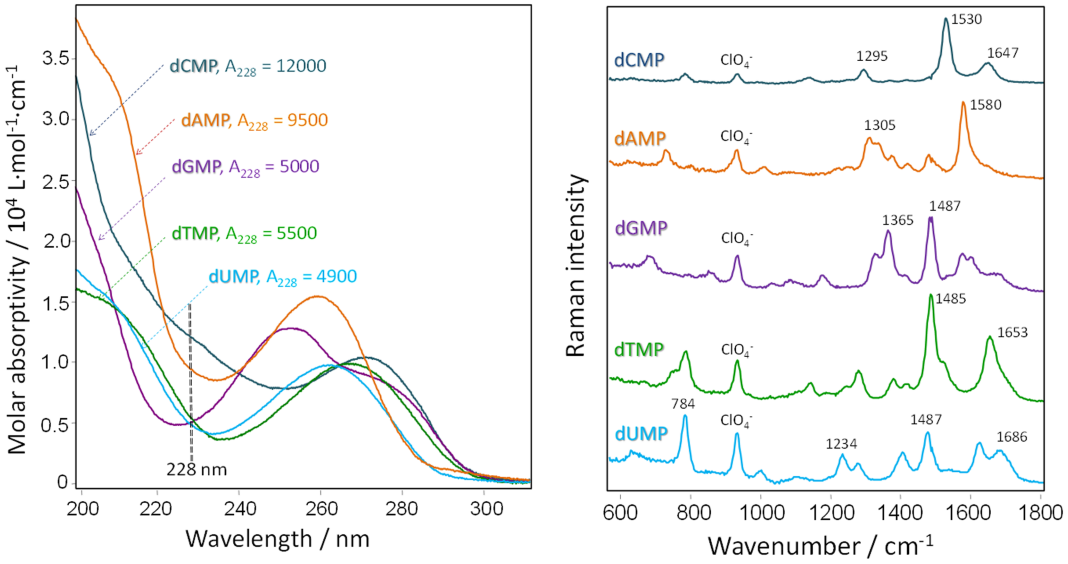

FIGURE 5 (a) DUV absorption and (b) 228-nm UVRR spectra (1 mg/mL, 30 s accumulation times) of nucleotides: dAMP, dCMP, dGMP, dTMP, and dUMP. A_{228} is the molar absorptivity at the 218-nm Raman excitation wavelength [Colour figure can be viewed at wileyonlinelibrary.com]

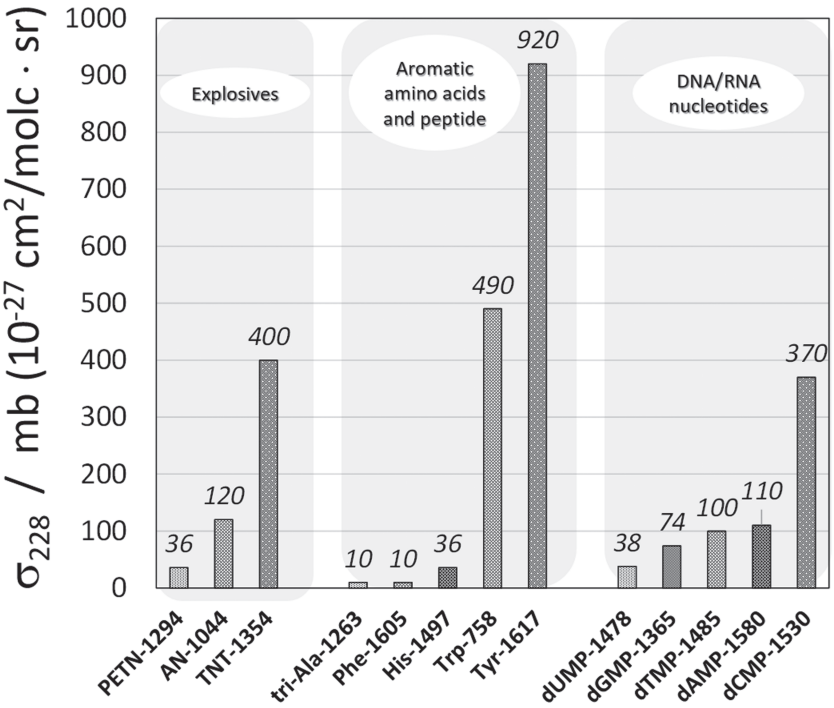

FIGURE 6 Comparison of the 228-nm absolute differential Raman cross sections of the most intense Raman bands of explosives, aromatic amino acids, peptides, and DNA/RNA nucleotides. Cross sections units are millibarns (mb) or 10^{-27} cm^2/molc·sr [Colour figure can be viewed at wileyonlinelibrary.com]

1354 cm^{-1}) = 400·10^{-27} cm^2/molc·sr or 400 millibarns (mb). PETN is the least enhanced. The 1294 cm^{-1} band cross section is approximately tenfold lower; σ_{228}(PETN, 1294) = 36 mb.

Previously, Ghosh et al[30] investigated excitation profiles of explosives in the DUV spectral region. They found that TNT and HMX Raman cross sections are maximized at ~230 nm. Therefore, 228-nm excitation is optimal for trace detection of TNT and HMX. In contrast, PETN, AN, and RDX have stronger electronic transitions deeper in the UV. These transitions can be excited by our recently developed compact 213-nm laser.[21]

Extensive studies of the aromatic amino acid excitation profiles show that 228 nm is very close to the maximal enhancement wavelength of Trp and Tyr[36,46,47]; 228-nm Trp and Tyr Raman cross sections are the highest among all of the compounds measured in this study, σ_{228}(Trp, 758) = 490 mb, σ_{228}(Tyr, 1617) = 920 mb. The Raman cross sections of His, Phe, and tri-Ala are more than tenfold lower (Figure 6 and Tables S4–S8).

Figure 4b shows the 228-nm UVRR spectrum of lysozyme (chicken egg white). The protein contains 147 amino acid residues including six Trp, three Tyr, four Phe, and one His. With 228-nm excitation, the UVRR spectrum of lysozyme is dominated by the vibrational modes of the Trp (759, 1010, 1350, 1551 cm^{-1}) and Tyr (1617 cm^{-1}) residues due to their large resonance enhancement.

The 228-nm Raman cross sections of the nucleotides' most intense bands are within tenfold of each other. dCMP shows the highest cross section, σ_{228}(dCMP, 1530) = 370 mb, similar to Trp. dUMP is the least enhanced, σ_{228}(dUMP, 1478) = 38 mb. Raman intensities of dAMP, dGMP, dTMP, and dUMP are approximately tenfold lower than Trp and Tyr.

Tyr, Trp, and dCMP are the most enhanced biological DUV chromophores with 228-nm Raman excitation.

5 | SUMMARY

We developed two compact 228-nm DUV laser light sources. These quadrupled quasi-three-level Nd:$GdVO_4$ DPSS lasers generate up to ~50 mW of 228-nm quasi-CW light as ns pulses at kilohertz repetition rates. These new lasers are of high utility for numerous UVRR applications because 228-nm excitation is in resonance with numerous DUV chromophores.

We used this laser to measure 228-nm absolute differential Raman cross section of explosives, peptides, aromatic amino acids, and DNA/RNA nucleotides.

The 228-nm Raman excitation overlaps with the $\pi \rightarrow \pi^*$ electronic transitions associated with conjugated double bonds, aromatic rings, amides, NO_x-compounds and other DUV chromophores. These 228-nm lasers can be used for standoff Raman monitoring of trace explosives. They also excite in a region that is sensitive to the molecular structure of many biological molecules such as

aromatic amino acids, DNA/RNA nucleotides, peptides, and proteins.

ACKNOWLEDGEMENT

We gratefully acknowledge funding from ONR Grant N00014-18-1-2072.

ORCID

Sergei V. Bykov https://orcid.org/0000-0002-6161-0027
Ryan D. Roppel https://orcid.org/0000-0002-1782-1388
Michael Mao https://orcid.org/0000-0003-4880-2371
Sanford A. Asher https://orcid.org/0000-0003-1061-8747

REFERENCES

[1] S. A. Oladepo, K. Xiong, Z. Hong, S. A. Asher, J. Handen, I. K. Lednev, *Chem. Rev. (Washington, DC, U. S.)* **2012**, *112*, 2604.
[2] G. Balakrishnan, C. L. Weeks, M. Ibrahim, A. V. Soldatova, T. G. Spiro, *Curr. Opin. Struct. Biol.* **2008**, *18*, 623.
[3] R. S. Jakubek, J. Handen, S. E. White, S. A. Asher, I. K. Lednev, *TrAC, Trends Anal. Chem.* **2018**, *103*, 223.
[4] Y. Kumamoto, A. Taguchi, S. Kawata, *Adv. Opt. Mater.* **2019**, *7*, 1801099.
[5] U. Neugebauer, P. Rösch, J. Popp, *Int. J. Antimicrob. Agents* **2015**, *46*, S35.
[6] C. Domes, R. Domes, J. Popp, M. W. Pletz, T. Frosch, *Anal. Chem. (Washington, DC, U. S.)* **2017**, *89*, 9997.
[7] S. R. Khandasammy, M. A. Fikiet, E. Mistek, Y. Ahmed, L. Halamkova, J. Bueno, I. K. Lednev, *Forensic Chem.* **2018**, *8*, 111.
[8] V. D'Elia, G. Montalvo, C. G. Ruiz, V. V. Ermolenkov, Y. Ahmed, I. K. Lednev, *Spectrochim. Acta, Part A* **2018**, *188*, 338.
[9] K. L. Gares, K. T. Hufziger, S. V. Bykov, S. A. Asher, *J. Raman Spectrosc.* **2016**, *47*, 124.
[10] A. J. Hopkins, J. L. Cooper, L. T. M. Profeta, A. R. Ford, *Appl. Spectrosc.* **2016**, *70*, 861.
[11] K. T. Hufziger, S. V. Bykov, S. A. Asher, *Appl. Spectrosc.* **2017**, *71*, 173.
[12] B. Rossi, S. Catalini, C. Bottari, A. Gessini, C. Masciovecchio, Frontiers of UV resonant raman spectroscopy by using synchrotron radiation: the case of aqueous solvation of model peptides, in *UV and Higher Energy Photonics: From Materials to Applications 2019*, Vol. 11086, International Society for Optics and Photonics 110860N.
[13] C. Bottari, I. Mancini, A. Mele, A. Gessini, C. Masciovecchio, B. Rossi, Conformational stability of DNA in hydrated ionic liquid by synchrotron-based UV resonance raman, in *UV and Higher Energy Photonics: From Materials to Applications 2019*, Vol. 11086, International Society for Optics and Photonics 110860Q.
[14] S. A. Asher, C. R. Johnson, J. Murtaugh, *Rev. Sci. Instrum.* **1983**, *54*, 1657.
[15] C. M. Jones, V. L. Devito, P. A. Harmon, S. A. Asher, *Appl. Spectrosc.* **1987**, *41*, 1268.
[16] S. A. Asher, R. W. Bormett, X. G. Chen, D. H. Lemmon, N. Cho, P. Peterson, M. Arrigoni, L. Spinelli, J. Cannon, *Appl. Spectrosc.* **1993**, *47*, 628.
[17] J. S. W. Holtz, R. W. Bormett, Z. Chi, N. Cho, X. G. Chen, V. Pajcini, S. A. Asher, L. Spinelli, P. Owen, M. Arrigoni, *Appl. Spectrosc.* **1996**, *50*, 1459.
[18] M. C. Sparrow, J. F. Jackovitz, C. H. Munro, W. F. Hug, S. A. Asher, *Appl. Spectrosc.* **2001**, *55*, 66.
[19] W. J. Abbey, R. Bhartia, L. W. Beegle, L. DeFlores, V. Paez, K. Sijapati, S. Sijapati, K. Williford, M. Tuite, W. Hug, R. Reid, *Icarus* **2017**, *290*, 201.
[20] S. Bykov, I. Lednev, A. Ianoul, A. Mikhonin, C. Munro, S. A. Asher, *Appl. Spectrosc.* **2005**, *59*, 1541.
[21] S. V. Bykov, M. Mao, K. L. Gares, S. A. Ashera, *Appl. Spectrosc.* **2015**, *69*, 895.
[22] A. I. Zagumennyi, V. G. Ostroumov, I. A. Shcherbakov, T. Jensen, J. P. Meyen, G. Huber, *Kvantovaya Elektron. (Moscow)* **1992**, *19*, 1149.
[23] A. Zagumennyi, V. Mikhailov, I. Shcherbakov, In *Handbook of Laser Technology and Applications*. **2004**; Vol. 2, p 353.
[24] T. Jensen, V. G. Ostroumov, J. P. Meyn, G. Huber, A. I. Zagumennyi, I. A. Shcherbakov, *Appl. Phys. B: Lasers Opt.* **1994**, *B58*, 373.
[25] Y. D. Zavartsev, A. I. Zagumennyi, F. Zerrouk, S. A. Kutovoi, V. A. Mikhailov, V. V. Podreshetnikov, A. A. Sirotkin, I. A. Shcherbakov, *Quantum Electron.* **2003**, *33*, 651.
[26] F. Chen, J. Sun, R. Yan, X. Yu, *Sci. Rep.* **2019**, *9*, 1.
[27] F. Chen, X. Yu, X. Li, R. Yan, C. Wang, M. Luo, J. Peng, Z. Zhang, J. Yu, *Opt. Commun.* **2010**, *283*, 3755.
[28] A. B. Zrimsek, S. V. Bykov, S. A. Asher, *Appl. Spectrosc.* **2019**, *73*, 601.
[29] J. M. Dudik, C. R. Johnson, S. A. Asher, *The Journal of Chemical Physics* **1985**, *82*, 1732.
[30] M. Ghosh, L. Wang, S. A. Asher, *Appl. Spectrosc.* **2012**, *66*, 1013.
[31] A. C. Albrecht, M. C. Hutley, *The Journal of Chemical Physics* **1971**, *55*, 4438.
[32] A. K. Chaudhary, A. M. Rudra, P. Kumbhakar, G. C. Bhar, *J. Appl. Spectrosc.* **2007**, *74*, 571.
[33] V. Tomisic, V. Butorac, J. Viher, V. Simeon, *J. Solution Chem.* **2005**, *34*, 613.
[34] P. A. Mullen, M. K. Orloff, *J. Phys. Chem.* **1973**, *77*, 910.
[35] D. D. Tuschel, A. V. Mikhonin, B. E. Lemoff, S. A. Asher, *Appl. Spectrosc.* **2010**, *64*, 425.
[36] S. A. Asher, M. Ludwig, C. R. Johnson, *J. Am. Chem. Soc.* **1986**, *108*, 3186.
[37] D. S. Caswell, T. G. Spiro, *J. Am. Chem. Soc.* **1986**, *108*, 6470.
[38] V. A. Bloomfield, D. M. Crothers, I. Tinoco, *Nucleic Acids: Structures, Properties, and Functions*, University Science Books, Sausalito, CA **2000**.
[39] A. Rodger, in *Encyclopedia of Biophysics*, (Ed: G. C. K. Roberts), Springer Berlin Heidelberg, Berlin, Heidelberg **2013** 2714.
[40] S. P. A. Fodor, R. P. Rava, T. R. Hays, T. G. Spiro, *J. Am. Chem. Soc.* **1985**, *107*, 1520.
[41] W. L. Kubasek, B. Hudson, W. L. Peticolas, *Proc. Natl. Acad. Sci. U. S. a.* **1985**, *82*, 2369.
[42] J. R. Perno, C. A. Grygon, T. G. Spiro, *J. Phys. Chem.* **1989**, *93*, 5672.
[43] M. Tsuboi, Y. Nishimura, A. Y. Hirakawa, In *Biological Applications of Raman Spectroscopy*; T. G. Spiro, Ed. Wiley-Interscience: New York, **1987**; vol. 2, pp. 109.
[44] M. Tsuboi, M. Komatsu, J. Hoshi, E. Kawashima, T. Sekine, Y. Ishido, M. P. Russell, J. M. Benevides, G. J. Thomas, *J. Am. Chem. Soc.* **1997**, *119*, 2025.

[45] L. Nagli, M. Gaft, Y. Fleger, M. Rosenbluh, *Opt. Mater.* **2008**, *30*, 1747.
[46] M. Ludwig, S. A. Asher, *J. Am. Chem. Soc.* **1988**, *110*, 1005.
[47] S. P. A. Fodor, R. A. Copeland, C. A. Grygon, T. G. Spiro, *J. Am. Chem. Soc.* **1989**, *111*, 5509.

SUPPORTING INFORMATION

Additional supporting information may be found online in the Supporting Information section at the end of this article.

How to cite this article: Bykov SV, Roppel RD, Mao M, Asher SA. 228-nm quadrupled quasi-three-level Nd:$GdVO_4$ laser for ultraviolet resonance Raman spectroscopy of explosives and biological molecules. *J Raman Spectrosc*. 2020;51:2478–2488. https://doi.org/10.1002/jrs.5999